

Quantification of liver and muscular fat using contrast-enhanced Dual Source Dual Energy Computed Tomography compared to an established multi-echo Dixon MRI sequence

Sebastian Gassenmaier^a, Karin Kähm^a, Sven S. Walter^a, Jürgen Machann^{b, c, d}, Konstantin Nikolaou^a, Malte N. Bongers^{a, *}

^a Department of Diagnostic and Interventional Radiology, Eberhard-Karls-University Tuebingen, Tuebingen, Germany

^b Section of Experimental Radiology, Department of Diagnostic and Interventional Radiology, Eberhard-Karls-University Tuebingen, Tuebingen, Germany

^c Institute for Diabetes Research and Metabolic Diseases of the Helmholtz Centre Munich at the University of Tübingen, Tübingen, Germany

^d German Center for Diabetes Research (DZD), Tübingen, Germany

ARTICLE INFO

Keywords:

Magnetic resonance imaging
Liver
Multidetector computed tomography
DECT

ABSTRACT

Purpose: To investigate the feasibility of liver fat quantification in contrast-enhanced dual source dual energy computed tomography (DECT) using multi-echo Dixon magnetic resonance imaging (MRI) as reference standard. **Method:** Patients who underwent MRI of the liver including a multi-echo Dixon sequence for estimation of proton density fat fraction in 2017 as well as contrast-enhanced DECT imaging of the abdomen were included in this retrospective, monocentric IRB approved study. Furthermore, patients with a hepatic fat amount >5% who were examined in 2018 with MRI and DECT were included. The final study group consisted of 81 patients with 90 pairs of examinations. Analysis of parameter maps was performed manually using congruent regions of interest which were placed in the liver parenchyma, in the erector spinae muscles, and psoas major muscles.

Results: Mean patient age was 61 ± 13 years. Median time between MRI and DECT was 48 days. MRI liver fat quantification resulted in a median of 3.8% (IQR: 2.2–8.2%) compared to 1.8% (IQR: 0–6.3%) in DECT ($p < 0.001$), with a Spearman correlation of 0.73. Bland-Altman analysis resulted in a systematic underestimation of liver fat in DECT, with a mean difference of -1.7% . Fat quantification in the erector spinae muscles ($p = 0.257$) and the psoas major muscles ($p = 0.208$) was not significantly different in DECT compared to MRI. **Conclusions:** Liver and muscular fat quantification in portal-venous phase DECT is feasible with good to excellent correlation compared to a multi-echo Dixon MRI sequence analysis. While there is an underestimation of the liver fat content in DECT, there are no significant differences between DECT and MRI fat quantification of the erector spinae and psoas major muscles.

1. Introduction

Increased fat content within liver parenchyma, known as hepatic steatosis, may lead to severe chronic liver diseases such as non-alcoholic fatty liver disease (NAFLD) [1,2]. NAFLD is a common illness with a prevalence ranging from 13 to 31% depending on the literature and geographic region [1,3]. Since NAFLD can progress to non-

alcoholic steatohepatitis (NASH) and thus increases the risk of liver cirrhosis, early diagnosis and monitoring is advisable [1,2]. In addition, it was previously shown that hepatic steatosis affects the outcome of patients after hepatic resection and transplantation [4,5]. One necessary criterion for the diagnosis of NAFLD is evidence of steatosis using imaging or biopsy [6]. Hepatic biopsy is currently regarded as reference

Abbreviations: NAFLD, Non-alcoholic fatty liver disease; NASH, Non-alcoholic steatohepatitis; US, Ultrasound; MRI, Magnetic resonance imaging; CT, Computed tomography; MRS, MR spectroscopy; PDFF, Proton-density fat fraction; SECT, Single energy CT; DECT, Dual energy CT; VIBE, Volumetric interpolated breath-hold examination; ROI, Region of interest; VNC, virtual non-contrast; HU, Hounsfield unit; SD, Standard deviation; IQR, Interquartile range

* Corresponding author at: Department of Diagnostic and Interventional Radiology, Eberhard-Karls-University Tuebingen, Hoppe-Seyler-Straße 3, 72076 Tuebingen, Germany.

E-mail address: malte.bongers@med.uni-tuebingen.de (M.N. Bongers).

<https://doi.org/10.1016/j.ejrad.2021.109845>

Received 12 May 2021; Received in revised form 17 June 2021; Accepted 2 July 2021

0720-048/© 2021

standard for fat quantification despite its invasiveness and the risk of sampling error [7–10].

Common imaging modalities involved in the assessment of steatosis are ultrasound (US), magnetic resonance imaging (MRI), and computed tomography (CT). Although, conventional US displays a well available and relatively cheap imaging technique, its major disadvantage is a primarily qualitative and not quantitative assessment of the liver fat content [11]. Another quantitative US technique is elastography, which is applied for the evaluation of liver fibrosis. However, data about quantitative fat measurement using US is still sparse [12,13]. MRI displays the most accurate imaging modality for quantitative fat evaluation of the liver, using MR spectroscopy (MRS) or by determination of the proton-density fat fraction (PDFF) [2,12]. A disadvantage of MRS is related to sampling error, whereas PDFF allows analysis of the whole liver parenchyma. The reliability and reproducibility of PDFF was also previously elaborated in several publications [14–16]. It was previously shown that liver attenuation in non-contrast CT is inversely correlated with the fat fraction of the organ, but can be unreliable in low degree steatosis and iron overload [11,17,18]. However, as contrast-enhanced CT is mostly used as primary imaging technique in clinical practice, liver attenuation is highly variable in single energy CT (SECT), due to alterations of the liver density depending on the contrast phase. The development of dual energy CT (DECT) provided the possibility of material decomposition based on different absorption characteristics of materials at different x-ray beam energies [19–21]. This allows to generate virtual unenhanced images with quantitative calculations of the iodine uptake and fat fraction quantification [19,21]. Liver fat quantification was investigated using dual energy technique in previous phantom and animal studies with promising results [22,23]. It was also shown by Hyodo et al. that hepatic fat quantification is feasible in humans with fast kilovolt peak switching DECT, with good correlation as compared to MR spectroscopy [7,24]. However, so far there is no comparison available of dual source DECT compared to a multi-echo Dixon MRI sequence.

Therefore, the aim of this study was to investigate the feasibility of liver fat quantification in contrast-enhanced dual source DECT, as compared to a multi-echo Dixon MRI sequence as standard of reference.

2. Materials and methods

2.1. Inclusion criteria

This retrospective, monocentric study was approved by the local institutional review board with waiver of informed consent. All patients who underwent a liver MRI including liver PDFF and iron analysis via LiverLab (Siemens Healthineers) at our institution during 2017 were searched via the radiology information system [16]. 557 examinations of 512 patients could be identified. A further inclusion criterion was contrast-enhanced DECT covering the whole liver within 6 months to the MRI examinations. This led to a drop-out of 444 patients. Thus, the study cohort of 2017 consisted of 68 patients with 74 pairs of examinations. Furthermore, to increase the number of patients with significant hepatic steatosis, patients with a hepatic fat amount above 5% determined by PDFF were included who were examined in 2018 with MRI as well as with DECT within 6 months to MRI. Sixteen patients with significant steatosis could be identified out of 64 patients with DECT and MRI. Therefore, the final study group for liver analysis resulted in 90 examinations of 81 patients.

2.2. MRI imaging protocol

All MRI examinations were performed using one of four clinical 1.5 or 3 Tesla scanners (Siemens MAGNETOM Avanto fit, Siemens MAGNETOM Aera, Siemens MAGNETOM Prisma fit, Siemens MAGNETOM Vida; all Siemens Healthineers). T1 weighted volumetric interpolated

breath-hold examination (VIBE) Dixon imaging of the upper abdomen was acquired including in- and opposed-phase imaging as well as calculation of fat and water selective images. Additionally, a multi-echo Dixon sequence was acquired for further tissue characterization to determine liver PDFF and to estimate iron load as previously described [16]. See Table 1 for MRI acquisition parameters.

2.3. Computed tomography imaging protocol

All DECT examinations were acquired using a 3rd generation dual source scanner (Siemens SOMATOM Force; Siemens Healthineers). After scout acquisition, imaging was conducted in a supine position and cranio-caudal scanning direction. Image datasets were acquired with a delay of 80 s after application of a non-ionic iodine contrast agent (iomeprol; Imeron 400; Bracco), which was adapted to patients' body weight (1 ml/kg) and followed by a saline flush of 30 ml. The dual energy imaging protocol consisted of a collimation of 0.6 mm as well as of a tube voltage of 100/Sn150 kV and a reference tube current of 190/95 mAs using automatic tube current modulation (CARE Dose; Siemens Healthineers). Mean CTDI_{vol} was 9.2 ± 2.5 mGy. Imaging reconstruction was performed using a soft tissue kernel (Qr40d) in axial and coronal plane with a slice thickness of 1.5 mm.

2.4. Image evaluation

All MRI studies were evaluated with commercially available post-processing software (Syngo.Via; Siemens Healthineers). Measurements were performed in consensus reading by two radiologists with three and eight years of experience in dual energy analysis. For liver PDFF quantification, the mean value of three regions of interest (ROI) which were manually drawn into the liver parenchyma (segment II/III, segment IVa/b, and segment VI/VII) of the fat fraction maps, which are automatically calculated by the software of the respective scanner, was calculated. No ROI was drawn into a focal liver lesion or into vessels. Similar to previous publications, a ROI size of 2.0 cm² was used within the liver [7]. Additionally, as iron deposits within liver parenchyma display a possible confounder for DECT fat quantification, liver iron content was evaluated in MRI by determination of the effective transversal relaxation rate R2* in the respective R2*-map using the same three ROIs as for fat quantification. Due to possible therapy-associated effects on the fat content of the liver parenchyma in the period between DECT and MRI, further measurements on less sensitive muscle and subcutaneous fat tissue were carried out in the patient cohort of the year 2017. Therefore, ROIs were placed into the left and right erector spinae muscles as well as the left and right psoas major muscles encompassing the whole muscle tissue on an axial slice. Additionally, another ROI was drawn into the subcutaneous fat tissue ventral of the right rectus abdominis muscle.

All DECT studies were further analyzed with commercially available post-processing software (Syngo.Via; Siemens Healthineers). Due to the different absorption spectrum of materials at different x-ray beam energies a fat map and virtual non-contrast (VNC) images were created us-

Table 1
MRI acquisition parameters.

	1.5 T	3 T
TE (ms)	1.09; 2.46; 3.69; 4.92; 6.15; 7.38	1.05; 2.46; 3.69; 4.92; 6.15; 7.38
TR (ms)	9	9
Flip angle (°)	4	4
Matrix	101x160	101x160
Voxel size (mm)	1.2 × 1.2 × 3.0	1.2 × 1.2 × 3.0
Slice thickness (mm)	3	3

Abbreviations: TE: echo time; TR: repetition time

ing DECT-source data. Similar to the evaluation of the MRI examinations three ROIs were manually drawn into liver segments, II/III, IVa/b, and VI/VII avoiding focal liver lesions and vessels in the same position as performed in MRI. The post-processing software provided the fat fraction as well as the VNC Hounsfield units (HU). The mean value of the three ROIs was used for correlation and comparison with MRI.

Additional ROIs in muscles and subcutaneous fat tissue were placed in the same anatomical structures in DECT imaging as described for MRI analysis. Bony landmarks (lumbar vertebral bodies) were used to identify the same position in MRI and DECT. Fat quantification values above 100% were set to 100% and negative values were set to 0%. See Figs. 1 and 2 for exemplary measurements.

To estimate the impact of therapy and environmental factors on liver fat deposition, a further subset of 17 pairs of examinations of MRI and DECT which were performed within one week was evaluated. Additionally, a subset of 37 cases with hepatic steatosis above 5% determined by PDFF was compared.

2.5. Statistical analysis

Proprietary statistical software was used for evaluation (SPSS Statistics Version 26, IBM). Parametric variables are displayed with

mean \pm standard deviation (SD). Non-parametric data are displayed using median and interquartile range (IQR) in parentheses. For paired data, the dependent *t*-test and the paired Wilcoxon signed rank-test were applied. Spearman correlation was used for the analysis of the MRI and DECT values. The significance level alpha was set at 0.05.

3. Results

3.1. Patients' characteristics

Mean patient age was 61 ± 13 years at MRI examination. Median time span between MRI and DECT imaging was 48 days (IQR 11–97 days). Liver fat amount (MRI PDFF) above 5% was found in 37 cases and above 10% in 14 cases. The indication for MRI and CT imaging was most often staging due to malignant disease. There was no significant difference between patients' body mass index between MRI (25.5 ± 3.9 kg/m²) and DECT (25.5 ± 4.0 kg/m²) ($p = 0.402$). Further patients' characteristics are displayed in Table 2.

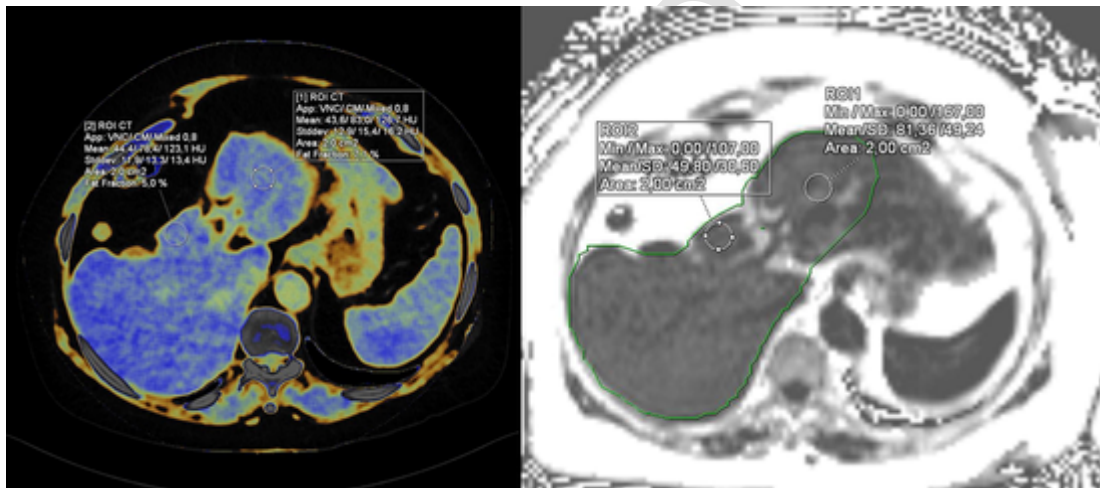


Fig. 1. Liver fat quantification using regions of interest with an area of 2.0 cm². MRI fat quantification resulted in 8.1% in segments II/III (DECT: 7.1%) and 5.0% in segment IV (DECT: 5.0%).

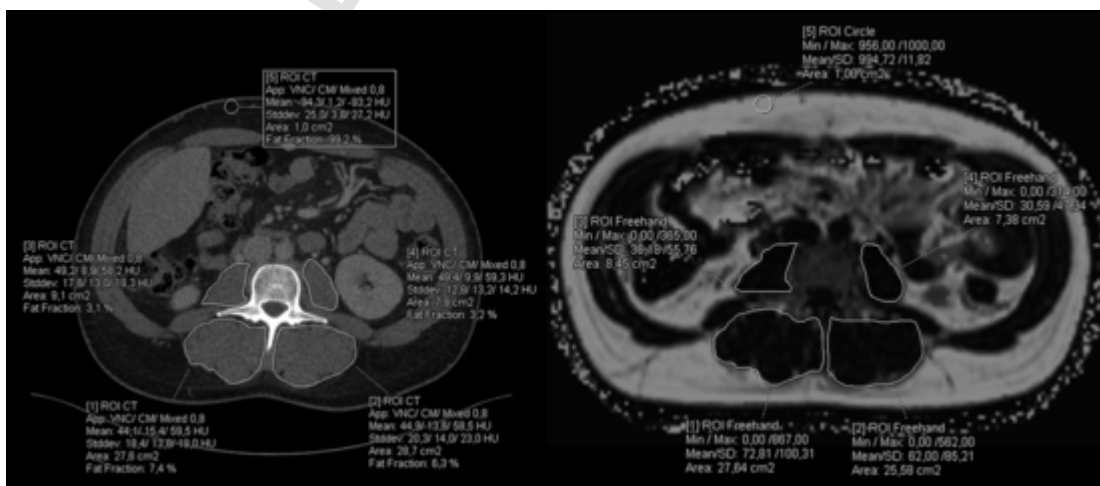


Fig. 2. Muscular and subcutaneous tissue fat quantification using DECT and MRI. Fat quantification results in similar values regarding the tissues of the erector spinae and psoas major muscles as well as regarding subcutaneous fat tissue: left psoas major muscle, MRI: 3.1%, DECT: 3.2%; right psoas major muscle, MRI: 3.6%, DECT: 3.1%; left erector spinae muscles, MRI: 6.2%, DECT: 6.3%; right erector spinae muscles, MRI: 7.3%, DECT: 7.4%; subcutaneous fat tissue, MRI: 99.5%, DECT: 99.2%.

Table 2
Patients' characteristics.

Characteristics	Values
Patients	n = 81
Examinations	n = 90
Mean age ± std.	61 ± 13 years
Range	23–87 years
Time period MRI – DECT	48 days (IQR 11–97 days)
<i>Indication for MRI and CT imaging</i>	
Carcinoma	n = 79 (88%)
Post LTX	n = 5 (5.5%)
Non-malignant disease	n = 6 (6.5%)
<i>Liver MRI findings</i>	
Malignant liver lesion	n = 40 (44.5%)
Non-malignant liver findings	n = 26 (29%)
No liver findings	n = 24 (26.5%)
<i>Cancer related therapy during MRI and DECT</i>	
None	n = 51 (56.5%)
Monoclonal anti-body therapy	n = 13 (14.5%)
Cytoreductive chemotherapy	n = 8 (9%)
Hormone therapy	n = 8 (9%)
Surgical/interventional therapy	n = 6 (6.5%)
Kinase inhibitor	n = 4 (4.5%)

Abbreviations: LTX: liver transplantation.

3.2. Comparison of MR and DECT liver fat quantification

Median MRI liver fat fraction was 3.8% (IQR 2.2–8.2%) vs. 1.8% (IQR 0–6.3%) in DECT ($p < 0.001$; Table 3). There was a good correlation between MRI- and DECT-based liver fat fraction of 0.73 ($p < 0.001$; Fig. 3). Bland-Altman assessment showed a systematic underestimation of hepatic fat deposition using DECT with a mean difference of -1.7% ($p < 0.001$; Table 4; Fig. 4). Median VNC attenuation was 55.0 HU (IQR 39.3–60.0 HU). There was excellent correlation of -0.95 between DECT liver fat quantification and VNC values ($p < 0.001$). Correlation between MRI liver PDFF quantification and VNC values was -0.67 ($p < 0.001$; Table 5).

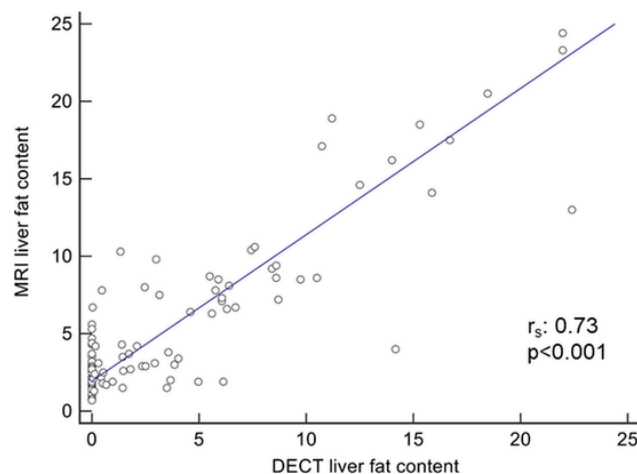
The subset analysis of 22 pairs of examinations which were performed within one week resulted in the following: steatosis above 5% ($< 10\%$) was found in four cases and steatosis above 10% in four cases. Correlation of determined DECT and MRI hepatic fat fraction was 0.88 ($p < 0.001$). However, MRI and DECT values were significantly different with a median MRI value of 3.3% (IQR 2.4–7.6%) and 1.4% (IQR 0–9.0%) for DECT ($p = 0.003$).

A second subset analysis was performed of all MRI and DECT examinations revealing a hepatic fat content above 5% in PDFF ($n = 37$). Liver fat amount was significantly different with a median of 8.6% (IQR 7.3–14.4%) in MRI and 7.4% (5.1–11.9%) in DECT ($p < 0.001$). Correlation between MRI and DECT was 0.77 ($p < 0.001$).

Table 3
Comparison of MRI and DECT fat quantification (values in percent).

	Median (IQR) MRI fat deposition	Median (IQR) DECT fat deposition	Median difference	Median absolute difference	p-value
Liver ($n = 90$)	3.8 (2.2–8.2)	1.8 (0–6.3)	-1.8	2.0	< 0.001
Left and right psoas major muscles ($n = 74$)	4.8 (3.4–6.4)	5.3 (3.2–7.8)	0.4	1.2	0.208
Left and right erector spinae muscles ($n = 74$)	11.9 (6.7–16.7)	12.6 (7.0–18.2)	0.1	1.3	0.257
Subcutaneous fat tissue ($n = 74$)	100 (99.9–100)	100 (100–100)	0.0	0.0	0.377

Abbreviations: IQR: interquartile range.

**Fig. 3.** Shows correlation statistics between MRI and DECT liver fat content. Spearman correlation resulted in 0.73 ($p < 0.001$).**Table 4**
Bland-Altman analysis of MRI and DECT fat quantification (values in percent).

	Mean difference	95% confidence interval	95% limits of agreement
Liver ($n = 90$)	-1.7	-2.3 to (-1.1)	-7.3 to 3.9
Left and right psoas major muscles ($n = 74$)	0.4	-0.1 to 1.0	-4.5 to 5.4
Left and right erector spinae muscles ($n = 74$)	0.5	-0.1 to 1.1	-4.3 to 5.3
Subcutaneous fat tissue ($n = 74$)	-0.3	-0.9 to 0.3	-5.4 to 4.9

3.3. Reference measurements of muscles and subcutaneous fat tissue in 2017 cohort ($n = 74$)

There was no significant difference between MRI and DECT fat quantification neither for the erector spinae and psoas major muscles nor the subcutaneous fat tissue (Fig. 4). Further details are displayed in Table 3 and 4. Correlation between MRI and DECT fat values ranged from 0.56 (subcutaneous fat) to 0.95 (erector spinae muscles; Table 5; Fig. 5). Median VNC attenuation was 46.9 HU (IQR 42.4–50.1 HU) for psoas major muscles, 35.9 HU (IQR 28.3–44.1 HU) for erector spinae muscles and -106.0 HU (IQR -108.4 to -101.7 HU) for subcutaneous fat tissue. Correlation between DECT fat quantification and VNC values was excellent for all muscle measurements ranging from -0.93 (left and right psoas major muscles) to -0.97 (left and right erector spinae muscles; all $p < 0.001$). Correlation between MRI muscle fat quantification and VNC values ranged from -0.77 (left and right psoas major muscles) to -0.91 (left and right erector spinae muscles; all $p < 0.001$; Table 5).

3.4. MRI quantification of hepatic iron deposits

Median $R2^*$ was 38.4 s^{-1} (ranging from 27.0 to 102.4) for 1.5 T and 48.2 s^{-1} (ranging from 26.4 to 142.4) for 3.0 T displaying no severe iron deposits [16,25,26]. Iron quantification via DECT was not possible as no non-contrast datasets were available.

4. Discussion

This study compared the accuracy of hepatic fat quantification based on DECT post-processing, as compared to an established multi-echo Dixon MRI sequence performing as reference standard. Our results show a good to excellent correlation for fat quantification between DECT and MRI. However, fat quantification of liver parenchyma in DECT demonstrated a systematic underestimation of -1.7% . The refer-

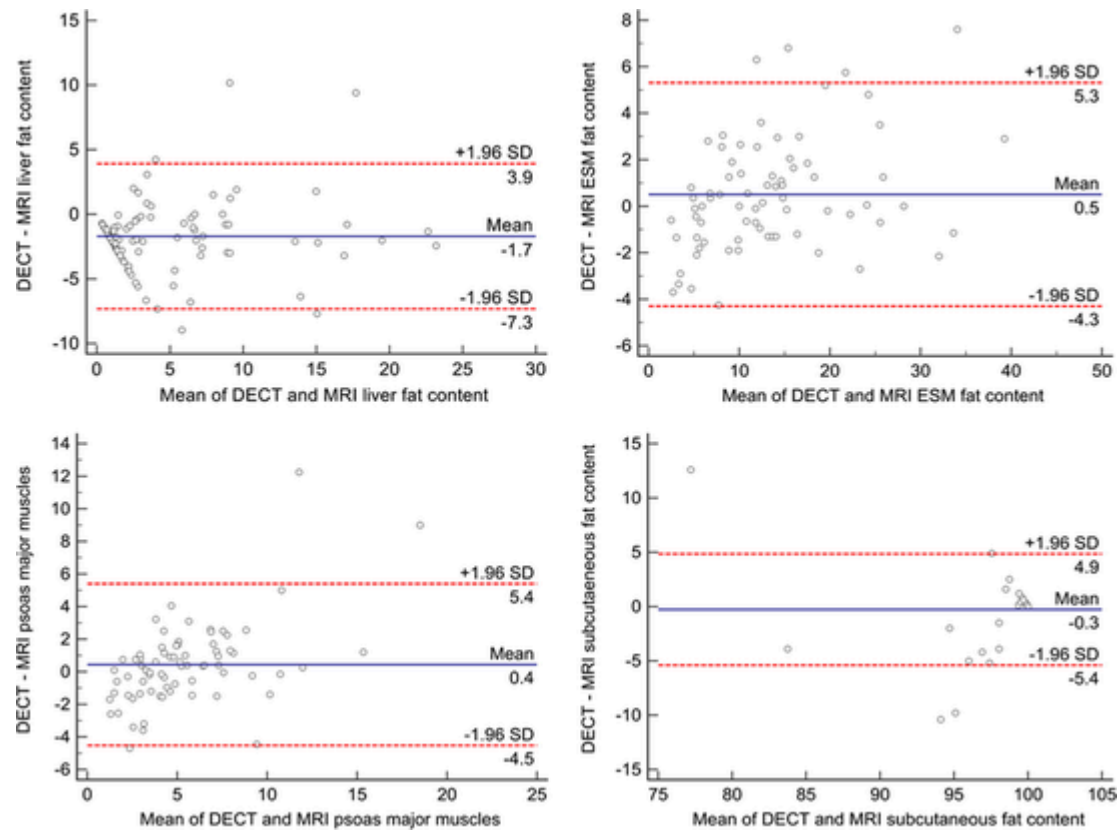


Fig. 4. Shows Bland-Altman plots for comparison of MRI and DECT fat quantification in liver, erector spinae muscles, psoas major muscles, and subcutaneous fat tissue. Abbreviations: ESM: erector spinae muscles.

Table 5

Correlation analysis of fat quantification in DECT and MRI as well as VNC values.

	Correlation	p-value
<i>Fat quantification MRI - DECT</i>		
Liver (n = 90)	0.73	<0.001
Left and right psoas major muscles (n = 74)	0.79	<0.001
Left and right erector spinae muscles (n = 74)	0.95	<0.001
Subcutaneous fat tissue (n = 74)	0.56	0.001
<i>DECT - VNC</i>		
Liver (n = 90)	-0.95	<0.001
Left and right psoas major muscles (n = 74)	-0.93	<0.001
Left and right erector spinae muscles (n = 74)	-0.97	<0.001
Subcutaneous fat tissue (n = 74)	-0.37	<0.001
<i>MRI - VNC</i>		
Liver (n = 90)	-0.67	<0.001
Left and right psoas major muscles (n = 74)	-0.77	<0.001
Left and right erector spinae muscles (n = 74)	-0.91	<0.001
Subcutaneous fat tissue (n = 74)	-0.25	0.029

Abbreviations: VNC: virtual non-contrast.

ence measurements performed in muscle and subcutaneous fat showed no significant differences between DECT and MRI and support the commonly known theory that liver fat content is influenced by numerous factors over time.

Interestingly, the results of this study showed better correlation between liver fat quantification of DECT and MRI compared to a previous study of Kramer et al. using non-contrast DECT datasets [12]. One reason for this could be due to technical nature, as the different findings might be related to the applied DECT technique and scanner generation. In the study of Kramer et al., a rapid kV switching method of 80/140 kV was applied compared to our dual source DECT approach with 100/Sn150 kV. Our findings are in line with the results of Hyodo et al.

who also determined a good agreement between DECT fat quantification and MR spectroscopy [7]. However, in contrast to Hyodo et al., image acquisition in the present study was performed in portal-venous phase using a 3rd generation dual source scanner instead of a fast kilovolt peak switching DECT. In both studies, Hyodo et al. as well as the present study, 150 kV was selected as the voltage level of the second tube. This might indicate that using higher tube voltages (150 kV vs. 140 kV) – especially in combination with additional tin filtration – might lead to better spectral separation and consecutively increased preciseness of liver fat quantification. Another reason may also be technical progress in scanner architecture with increased image quality. Recent research also indicates that radiomics analysis of DECT studies could be useful for tissue characterization of liver parenchyma showing that differentiation between normal liver, steatosis, and cirrhosis is possible [27].

Of course, the question of the clinical importance of these findings arises. Most CT examinations performed in clinical practice, e. g. for staging purposes, are acquired in portal-venous phase as multi-phase CT examinations are usually avoided due to radiation exposure. As this contrast-enhanced phase is of highest clinical significance, reliable fat quantification using portal-venous phase scans displays an important impact for patient management, especially as it was already previously shown that contrast-enhanced SECT studies are not adequately suitable for steatosis assessment [11]. Although our results indicate a slight underestimation of fat content of liver parenchyma, it is still possible to rule out or confirm steatosis. Reasons for this underestimation might be deposition of iron or copper, or other external environmental factors influencing liver parenchyma, especially since there was no significant difference in fat quantification regarding the muscle tissue. Furthermore, the subset analysis of liver fat quantification of our patients examined within seven days showed an excellent correlation between DECT and MRI. A possible method to compensate for this systematic

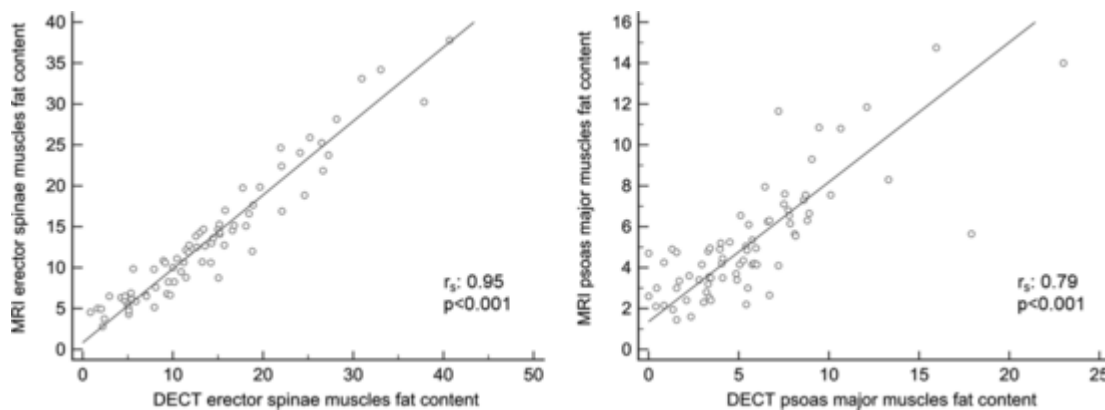


Fig. 5. Shows Spearman correlation statistics between MRI and DECT fat quantification in erector spinae muscles (0.95) and psoas major muscles (0.79) (both $p < 0.001$).

underestimation might display the usage of a correction factor for liver fat quantification in DECT.

This study has several limitations. First, the time period between MRI and DECT examinations. An influence of environmental factors on liver fat content between MRI and DECT imaging cannot be ruled out. Additionally, almost all patients suffered from a malignant primary disease with some patients receiving medication which may have had an influence on liver fat content [28]. Additionally, liver parenchyma is very sensitive to lifestyle changes, especially regarding nutrition [29]. Therefore, we performed the above-mentioned sub-analysis of patients who received imaging with both modalities within one week. Another step to compensate for this limitation displayed the measurements of the psoas major muscles and the erector spinae muscles, and the subcutaneous fat tissue as these tissues are less susceptible to medication. The increased agreement of the muscle measurements compared to the liver might fortify this approach. Another limitation that merits consideration consists of the iron deposits within the liver. Storage diseases leading to an increased liver content of iron or copper affect the liver attenuation values in CT imaging inversely to hepatic steatosis [22,30]. However, the MRI iron deposits analysis in our patient cohort showed no severe iron deposits within the liver parenchyma. Furthermore, only contrast-enhanced portal-venous phase DECT were analyzed in this study and no unenhanced scans. However, this is also a unique strength of this study as most abdominal DECT for staging purposes are acquired in portal-venous phase.

In conclusion, liver and muscular fat quantification in portal-venous phase DECT is feasible with good to excellent correlation compared to a multi-echo Dixon MRI sequence analysis. Our results indicate a slight underestimation of liver fat content compared to established multi-echo Dixon MRI. However, there was no significant difference between MRI and DECT regarding fat measurements in erector spinae and psoas major muscles as well as regarding the subcutaneous fat tissue indicating the important role of influencing cofactors like iron deposition and medical therapy regimens on liver fat content. A correction factor for liver fat content analysis via DECT might display a compensation method to avoid systematic underestimation.

CRediT authorship contribution statement

Sebastian Gassenmaier: Methodology, Formal analysis, Investigation, Data curation, Writing - original draft, Visualization, Project administration. **Karin Kähm:** Formal analysis, Investigation, Visualization, Conceptualization, Data curation, Writing - original draft. **Sven S. Walter:** Software, Resources, Writing - review & editing. **Jürgen Machann:** Software, Resources, Writing - review & editing. **Konstantin Nikolaou:** Resources, Project administration, Writing - review & editing. **Malte N.**

Bongers: Conceptualization, Methodology, Investigation, Validation, Formal analysis, Resources, Data curation, Writing - review & editing, Supervision, Project administration.

Declaration of Competing Interest

The authors declare that they have no known competing financial interests or personal relationships that could have appeared to influence the work reported in this paper.

References

- [1] N. Chalasani, Z. Younossi, J.E. Lavine, M. Charlton, K. Cusi, M. Rinella, S.A. Harrison, E.M. Brunt, A.J. Sanyal, The diagnosis and management of nonalcoholic fatty liver disease: Practice guidance from the American Association for the Study of Liver Diseases, *Hepatology* 67 (1) (2018) 328–357.
- [2] Y.N. Zhang, K.J. Fowler, G. Hamilton, J.Y. Cui, E.Z. Sy, M. Balanay, J.C. Hooker, N. Szevenyi, C.B. Sirlin, Liver fat imaging—a clinical overview of ultrasound, CT, and MR imaging, *Br. J. Radiol.* 91 (1089) (2018) 20170959.
- [3] Z.M. Younossi, A.B. Koenig, D. Abdelatif, Y. Fazel, L. Henry, M. Wymer, Global epidemiology of nonalcoholic fatty liver disease—Meta-analytic assessment of prevalence, incidence, and outcomes, *Hepatology* 64 (1) (2016) 73–84.
- [4] D.A. Kooby, Y. Fong, A. Suriawinata, M. Gonen, P.J. Allen, D.S. Klimstra, R.P. DeMatteo, M. D’Angelica, L.H. Blumgart, W.R. Jarnagin, Impact of steatosis on perioperative outcome following hepatic resection, *J. Gastrointest. Surg.* 7 (8) (2003) 1034–1044.
- [5] R.J. Ploeg, A.M. D’Alessandro, S.J. Knechtle, M.D. Stegall, J.D. Pirsch, R.M. Hoffmann, T. Sasaki, H.W. Sollinger, F.O. Belzer, M. Kalayoglu, Risk factors for primary dysfunction after liver transplantation—a multivariate analysis, *Transplantation* 55 (4) (1993) 807–813.
- [6] N. Chalasani, Z. Younossi, J.E. Lavine, A.M. Diehl, E.M. Brunt, K. Cusi, M. Charlton, A.J. Sanyal, The diagnosis and management of non-alcoholic fatty liver disease: practice Guideline by the American Association for the Study of Liver Diseases, American College of Gastroenterology, and the American Gastroenterological Association, *Hepatology* 55 (6) (2012) 2005–2023.
- [7] T. Hyodo, N. Yada, M. Hori, O. Maenishi, P. Lamb, K. Sasaki, M. Onoda, M. Kudo, T. Mochizuki, T. Murakami, Multimaterial Decomposition Algorithm for the Quantification of Liver Fat Content by Using Fast-Kilovolt-Peak Switching Dual-Energy CT: Clinical Evaluation, *Radiology* 283 (1) (2017) 108–118.
- [8] E. Fassio, E. Alvarez, N. Dominguez, G. Landeira, C. Longo, Natural history of nonalcoholic steatohepatitis: a longitudinal study of repeat liver biopsies, *Hepatology* 40 (4) (2004) 820–826.
- [9] R. Vuppalanchi, A. Unalp, M.L. Van Natta, O.W. Cummings, K.E. Sandrasegaran, T. Hameed, J. Tonascia, N. Chalasani, Effects of liver biopsy sample length and number of readings on sampling variability in nonalcoholic Fatty liver disease, *Clin. Gastroenterol. Hepatol.* 7 (4) (2009) 481–486.
- [10] A.A. Bravo, S.G. Sheth, S. Chopra, Liver biopsy, *N. Engl. J. Med.* 344 (7) (2001) 495–500.
- [11] Y. Kodama, C.S. Ng, T.T. Wu, G.D. Ayers, S.A. Curley, E.K. Abdalla, J.N. Vauthey, C. Charnsangavej, Comparison of CT methods for determining the fat content of the liver, *AJR Am. J. Roentgenol.* 188 (5) (2007) 1307–1312.
- [12] H. Kramer, P.J. Pickhardt, M.A. Kliever, D. Hernandez, G.H. Chen, J.A. Zagzebski, S. B. Reeder, Accuracy of Liver Fat Quantification With Advanced CT, MRI, and Ultrasound Techniques: Prospective Comparison With MR Spectroscopy, *AJR Am. J. Roentgenol.* 208 (1) (2017) 92–100.
- [13] W.K. Jeong, H.K. Lim, H.K. Lee, J.M. Jo, Y. Kim, Principles and clinical application of ultrasound elastography for diffuse liver disease, *Ultrasonography* 33 (3) (2014) 149–160.
- [14] C. Caussy, S.B. Reeder, C.B. Sirlin, R. Loomba, Noninvasive, Quantitative

- Assessment of Liver Fat by MRI-PDFF as an Endpoint in NASH Trials, *Hepatology* 68 (2) (2018) 763–772.
- [15] G.H. Kang, I. Cruite, M. Shiehmorteza, T. Wolfson, A.C. Gamst, G. Hamilton, M. Bydder, M.S. Middleton, C.B. Sirlin, Reproducibility of MRI-determined proton density fat fraction across two different MR scanner platforms, *J. Magn. Reson. Imaging* 34 (4) (2011) 928–934.
- [16] X. Zhong, M.D. Nickel, S.A. Kannengiesser, B.M. Dale, B. Kiefer, M.R. Bashir, Liver fat quantification using a multi-step adaptive fitting approach with multi-echo GRE imaging, *Magn. Reson. Med.* 72 (5) (2014) 1353–1365.
- [17] P. Limanond, S.S. Raman, C. Lassman, J. Sayre, R.M. Ghobrial, R.W. Busuttill, S. Saab, D.S. Lu, Macrovesicular hepatic steatosis in living related liver donors: correlation between CT and histologic findings, *Radiology* 230 (1) (2004) 276–280.
- [18] S.R. Mills, J.L. Doppman, A.W. Nienhuis, Computed tomography in the diagnosis of disorders of excessive iron storage of the liver, *J. Comput. Assist. Tomogr.* 1 (1) (1977) 101–104.
- [19] C.H. McCollough, S. Leng, L. Yu, J.G. Fletcher, Dual- and Multi-Energy CT: Principles, Technical Approaches, and Clinical Applications, *Radiology* 276 (3) (2015) 637–653.
- [20] T.R. Johnson, B. Krauss, M. Sedlmair, M. Grasruck, H. Bruder, D. Morhard, C. Fink, S. Weckbach, M. Lenhard, B. Schmidt, T. Flohr, M.F. Reiser, C.R. Becker, Material differentiation by dual energy CT: initial experience, *Eur. Radiol.* 17 (6) (2007) 1510–1517.
- [21] B. Kaltenbach, J.L. Wichmann, S. Pfeifer, M.H. Albrecht, C. Booz, L. Lenga, R. Hammerstingl, T. D'Angelo, T.J. Vogl, S.S. Martin, Iodine quantification to distinguish hepatic neuroendocrine tumor metastasis from hepatocellular carcinoma at dual-source dual-energy liver CT, *Eur. J. Radiol.* 105 (2018) 20–24.
- [22] M.A. Fischer, R. Gnannt, D. Raptis, C.S. Reiner, P.A. Clavien, B. Schmidt, S. Leschka, H. Alkadhi, R. Goetti, Quantification of liver fat in the presence of iron and iodine: an ex-vivo dual-energy CT study, *Invest. Radiol.* 46 (6) (2011) 351–358.
- [23] B. Wang, Z. Gao, Q. Zou, L. Li, Quantitative diagnosis of fatty liver with dual-energy CT. An experimental study in rabbits, *Acta Radiol.* 44 (1) (2003) 92–97.
- [24] T. Hyodo, M. Hori, P. Lamb, K. Sasaki, T. Wakayama, Y. Chiba, T. Mochizuki, T. Murakami, Multimaterial Decomposition Algorithm for the Quantification of Liver Fat Content by Using Fast-Kilovolt-Peak Switching Dual-Energy CT: Experimental Validation, *Radiology* 282 (2) (2017) 381–389.
- [25] J.S. Hankins, M.B. McCarville, R.B. Loeffler, M.P. Smeltzer, M. Onciu, F.A. Hoffer, C. S. Li, W.C. Wang, R.E. Ware, C.M. Hillenbrand, R2* magnetic resonance imaging of the liver in patients with iron overload, *Blood* 113 (20) (2009) 4853–4855.
- [26] P. Storey, A.A. Thompson, C.L. Carqueville, J.C. Wood, R.A. de Freitas, C.K. Rigsby, R2* imaging of transfusional iron burden at 3T and comparison with 1.5T, *J. Magn. Reson. Imaging* 25 (3) (2007) 540–547.
- [27] R. Doda Khera, F. Homayounieh, F. Lades, B. Schmidt, M. Sedlmair, A. Primak, S. Saini, M.K. Kalra, Can Dual-Energy Computed Tomography Quantitative Analysis and Radiomics Differentiate Normal Liver From Hepatic Steatosis and Cirrhosis?, *J. Comput. Assist. Tomogr.* 44 (2) (2020) 223–229.
- [28] A.S. Siddique, O. Siddique, M. Einstein, E. Urtasun-Sotil, S. Ligato, Drug and herbal/dietary supplements-induced liver injury: A tertiary care center experience, *World J. Hepatol.* 12 (5) (2020) 207–219.
- [29] M. Nouredin, A. Vipani, C. Bresee, T. Todo, I.K. Kim, N. Alkhouri, V.W. Setiawan, T. Tran, W.S. Ayoub, S.C. Lu, A.S. Klein, V. Sundaram, N.N. Nissen, NASH Leading Cause of Liver Transplant in Women: Updated Analysis of Indications For Liver Transplant and Ethnic and Gender Variances, *Am. J. Gastroenterol.* 113 (11) (2018) 1649–1659.
- [30] D.T. Boll, E.M. Merkle, Diffuse liver disease: strategies for hepatic CT and MR imaging, *Radiographics* 29 (6) (2009) 1591–1614.